ELECTRONIC SUPPLEMENTARY INFORMATION

Using chiral ammonium cations to modulate the structure of 1D hybrid lead bromide perovskites for linearly polarized broadband light emission at room temperature

Joanna M. Urban, Abdelaziz Jouaiti, Nathalie Gruber, Géraud Delport, Gaëlle Trippé-Allard, Jean-François Guillemoles, Emmanuelle Deleporte, Sylvie Ferlay and Damien Garrot

XRPD measurements

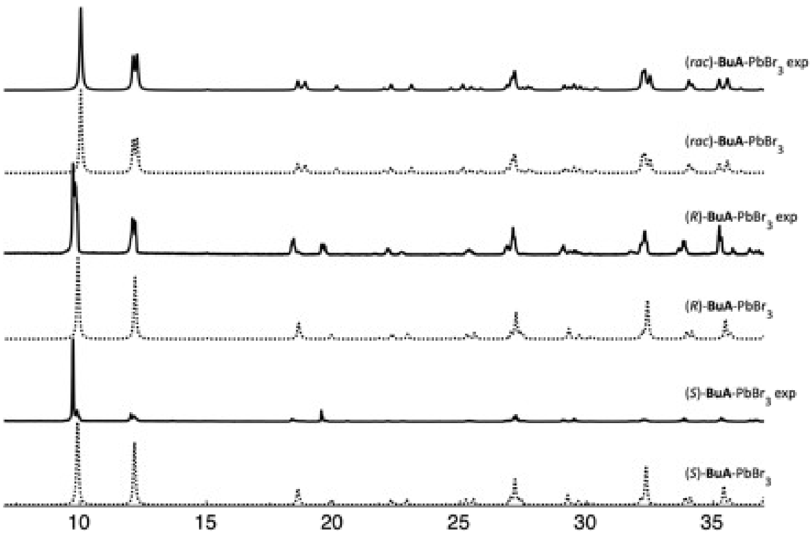

BUA-$PbBr_3$

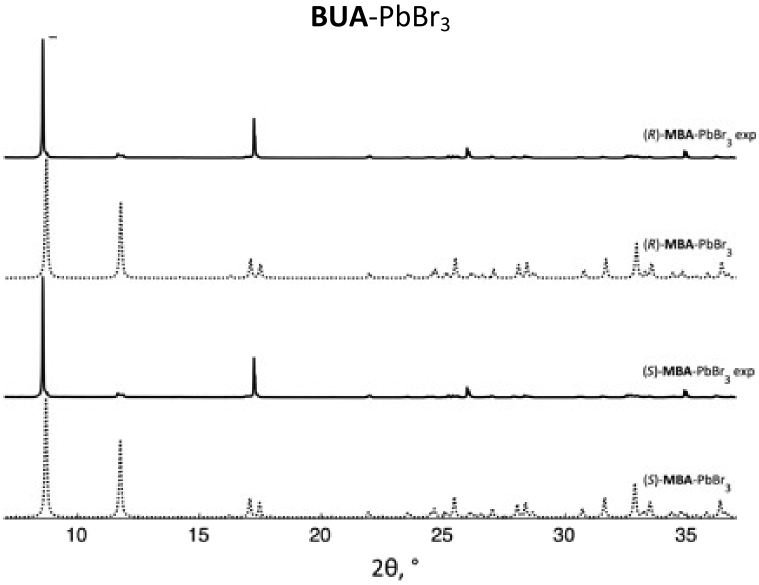

MBAH-$PbBr_3$

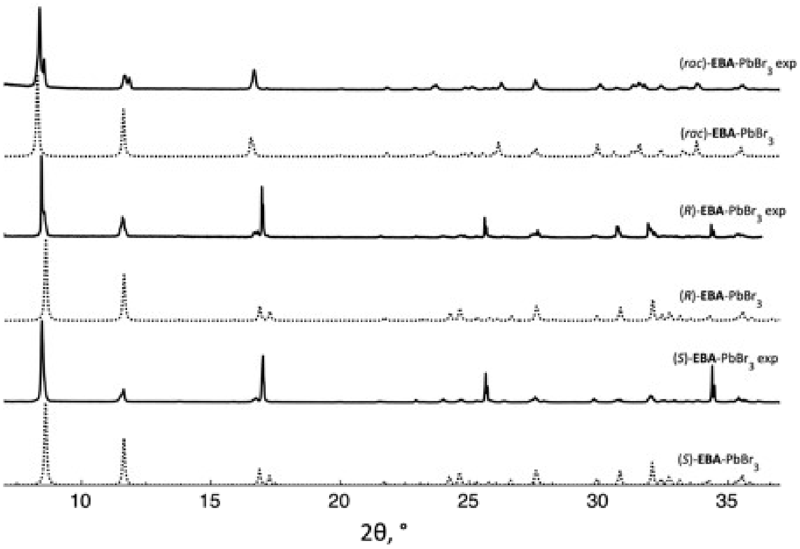

EBA-$PbBr_3$

Figure S1: For (*S*), (*R*) and (*rac*)-**BUA**-$PbBr_3$, *S*), (*R*) **MBA**H-$PbBr_3$ and (*S*), (*R*) and (*rac*)-**EBA**-$PbBr_3$**,** comparison of the simulated and experimental powder X-Ray diffraction studies (PXRD) diagrams

Optical absorption spectra

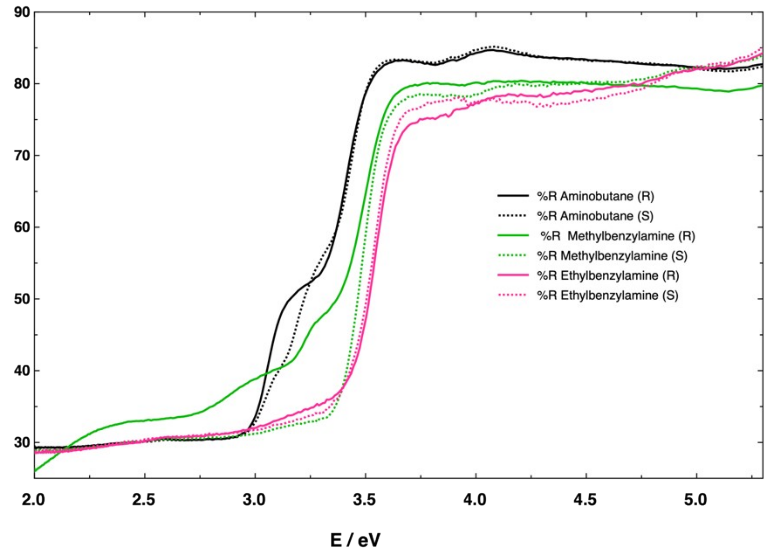

Figure S2: UV–vis diffuse reflectance spectra of the polycrystalline samples of (*S*)-**BuA**-$PbBr_3$, (S)-MBA-$PbBr_3$, (S)-**EBA**-$PbBr_3$, (*R*)-**BuA**-$PbBr_3$, (R)-**MBA**-$PbBr_3$, and (R)-**EBA**-$PbBr_3$

.

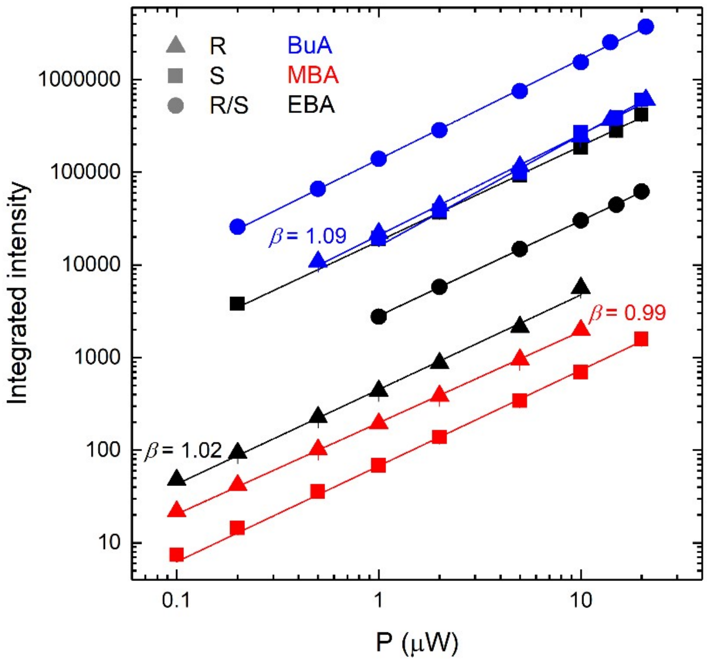

Figure S3: Integrated intensity of the broad emission peak as a function of the 3.06 eV excitation power for the massive crystal samples. The experimental data is marked in blue (**BuA**-$PbBr_3$), red (**MBA**-$PbBr_3$) and black (**EBA**-$PbBr_3$) circles (racemic mix), triangles (*R* enantiomer) and squares (*S* enantiomer). The lines show the fit of the power law $I=aP^{\beta}$, the coefficients β are marked for the three R-enantiomer samples. For the pure enantiomers the coefficients obtained were 1.09 and 1.20 (**BuA**-$PbBr_3$), 0.99 and 1.03 (**MBA**-$PbBr_3$), and 1.02 and 1.03 (**EBA**-$PbBr_3$) for R and S enantiomers, respectively.

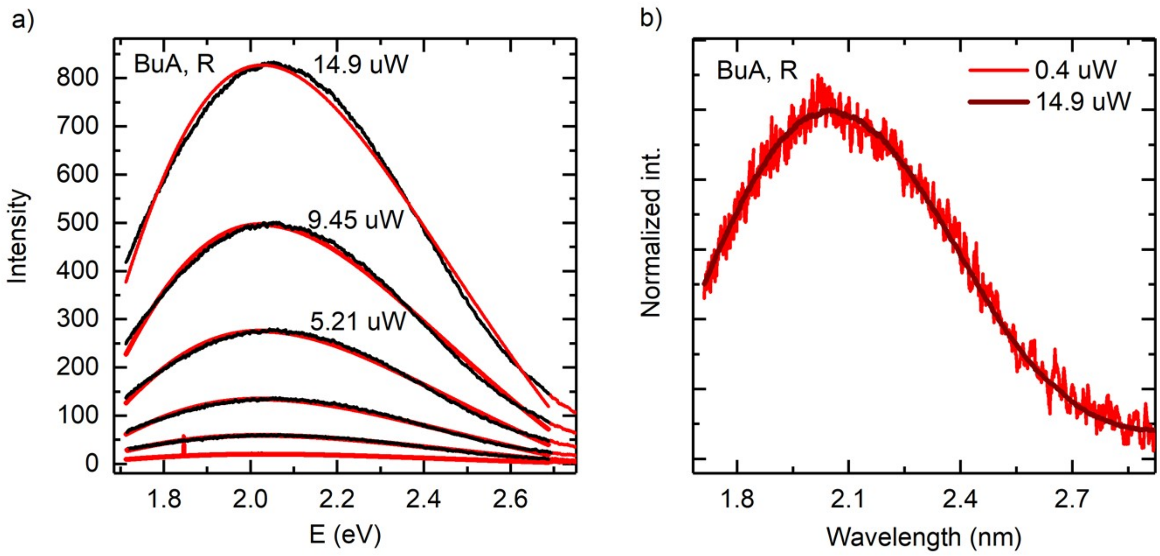

Figure S4: a) Photoluminescence spectra as a function of excitation power for the (*R*)-**BuA**-$PbBr_3$ compound for 405 nm (3.06 eV) excitation: spectra (black) and Gaussian fits (red) used to estimate the emission intensity. b) Normalized spectra at highest and lowest measured excitation power for the the (*R*)-**BuA**-$PbBr_3$ compound. No change of spectral shape is observed with increasing excitation power. Data is shown for one exemplary compound but the PL of the other compounds showed similar characteristics.

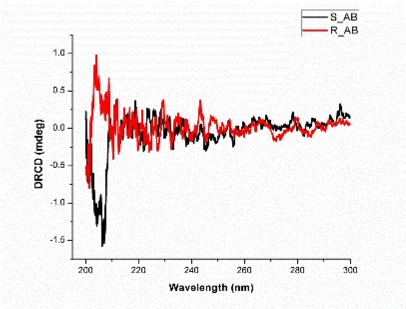

BUA-$PbBr_3$

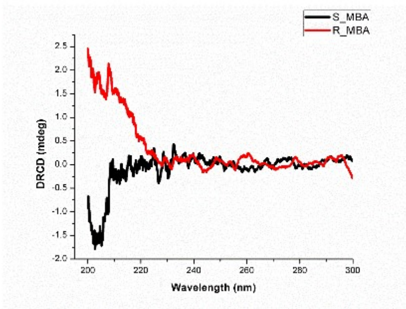

MBAH-$PbBr_3$

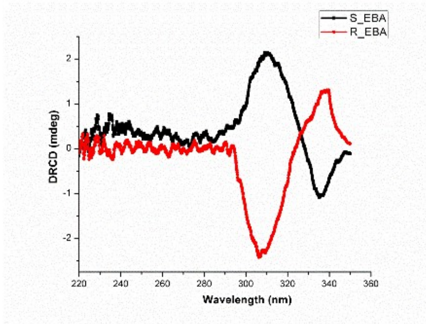

EBA-$PbBr_3$

Figure S5: Circular dichroism (reflectance) of the polycrystalline samples of (S) and (R)-**BuA**-$PbBr_3$, **MBA**-$PbBr_3$and **EBA**-$PbBr_3$

X-Ray data

	(*S*)-**BuA**-$PbBr_3$	(*R*)-**BuA**-$PbBr_3$	*rac*-**BuA**-$PbBr_3$	(*S*)-**MBA**-$PbBr_3$[1]	(*R*)-**MBA**-$PbBr_3$	(*S*)-**EBA**-$PbBr_3$	(*R*)-**EBA**-$PbBr_3$	*rac*-**EBA**-$PbBr_3$
Formula	$PbBr_3$, $C_4H_{12}N$	$PbBr_3$, $C_4H_{12}N$	$PbBr_3$, $C_4H_{12}N$	$PbBr_3$, $C_8H_{12}N$	$PbBr_3$, $C_8H_{12}N$	$PbBr_3$, $C_9H_{14}N$	$PbBr_3$, $C_9H_{14}N$	Pb2Br6, $C_9H_{13}N$
Molecular weight (gmol^{-1})	521.07	521.07	521.07	569.11	569.11	583.13	583.13	582.12
Crystal system	Orthorhombic	Orthorhombic	Monoclinic	Orthorhombic	Orthorhombic	Orthorhombic	Orthorhombic	Orthorhombic
Space group	$P2_12_12_1$	$P2_12_12_1$	$P2_1/n$	$P2_12_12_1$	$P2_12_12_1$	$P2_12_12_1$	$P2_12_12_1$	*P*nma
a(Å)	7.8629(6)	7.8483(3)	7.9713(7)	7.9016(5)	7.8860(4)	8.1770(4)	8.1743(4)	8.0192(7)
b(Å)	7.9677(7)	7.9539(3) Å	7.9713(7)	8.0986(4)	8.0842(4)	8.2177(4)	8.2125(4)	8.1450(6)
c(Å)	17.8420(13) Å	17.8105(8)	17.6232(13)	20.2960(12)	20.2617(9)	20.5239(10)	20.4992(12)	21.301(2)
α(deg)	90	90	90	90	90	90	90	90
β(deg)	90	90	90.932(4)	90	90	90	90	90
γ(deg)	90	90	90	90	90	90	90	90
V(Å^3)	1117.79(15)	1111.81(8)	1111.27(16)	1298.78(13)	1291.72(11)	1379.13(12)	1376.14(12	1391.3(2)
Z	4	4	4	4	4	4	4	4
Colour	Colourless	Colourless	Colourless	Colourless	Colourless	Colourless	Colourless	Colourless
Crystal dim (mm^3)	0.100 x 0.110 x 0.120	0.090 x 0.090 x 0.090	0.100 x 0.100 x 0.150	0.100 x 0.100 x 0.110	0.080 x 0.080 x 0.100	0.100 x 0.110 x 0.110	0.100 x 0.120 x 0.120	0.090 x 0.120 x 0.130
Dcalc (gcm^{-3})	3.096	3.113		2.910	2.926	2.808	2.815	2.779
F(000)	920	920	1524	1016	1016	1048	1048	1044
μ (mm^{-1})	25.756	25.894	31.515	22.181	22.302	20.892	20.937	20.709
Wavelength (Å)	0.71073	0.71073	0.71073	0.71073	0.71073	0.71073	0.71073	0.71073
Number of data meas.	6811	14387	10108	8107	104048	13637	15012	5225
Number of data with I> 2σ(I)	3257 [R(int) = 0.0612]	3178 [R(int) = 0.0831]	2658	3700 [R(int) = 0.0460]	3807 [R(int) = 0.0774]	4470 [R(int) = 0.0605]	4032 [R(int) = 0.0704]	1772 [R(int) = 0.0797]
R (%)	R1 = 0.0459, wR2 = 0.0953	R1 = 0.0349, wR2 = 0.0692	R1 = 0.0499, wR2 = 0.1291	0.0328, wR2 = 0.0695	R1 = 0.0165, wR2 = 0.0360	R1 = 0.0412, wR2 = 0.0998	R1 = 0.0410, wR2 = 0.0965	R1 = 0.0486, wR2 = 0.1123
Rw (%)	R1 = 0.0548, wR2 = 0.0980	R1 = 0.0402, wR2 = 0.0707	R1 = 0.0734, wR2 = 0.1506	0.0399, wR2 = 0.0720	R1 = 0.0181, wR2 = 0.0363	R1 = 0.0493, wR2 = 0.1026	R1 = 0.0513, wR2 = 0.1004	R1 = 0.0682, wR2 = 0.1227
GOF	1.057	0.921	0.871	0.935	1.308	1.080	1.031	1.095
Flack	0.013(17)	0.017(10)	-	-0.011(10)	0.023(4)	0.000(10)	-0.001(10)	-
Largest peak in final difference (eÅ^{-3})	1.843 and -1.869	2.015 and -2.608	1.982 and 2.638	2.054 and -1.855	1.273 and -0.562	2.507 and -2.409	2.235 and -1.816	2.721 and -2.607

Table S1. Crystallographic data for (*S*)-**BuA**-$PbBr_3$, (*R*)-**BuA**-$PbBr_3$, *rac*-**BuA**-$PbBr_3$, (*S*)-**MBA**-$PbBr_3$, (*R*)-**MBA**-$PbBr_3$, (*S*)-**EBA**-$PbBr_3$, (*R*)-**EBA**-$PbBr_3$ and *rac*-**EBA**-$PbBr_3$, measured at 100K

[1] Y. Dang, X. Liu, Y. Sun, J. Song, W. Hu, X. Tao Bulk Chiral Halide Perovskite Single Crystals for Active Circular Dichroism and Circularly Polarized Luminescence *J. Phys. Chem. Lett*. **2020**, *11*, 1689-1696

X-Ray data

	(*S*)-**BuA**-$PbBr_3$	(*R*)-**BuA**-$PbBr_3$	*rac*-**BuA**-$PbBr_3$	(*S*)-**MBA**-$PbBr_3$	(*R*)-**MBA**-$PbBr_3$	(*S*)-**EBA**-$PbBr_3$	(*R*)-**EBA**-$PbBr_3$	*rac*-**EBA**-$PbBr_3$
	2167654	2167649	2167653	2167650	2167652	2167655	2167656	2167651
d_{Pb-Br}	2.8461(15) 2.9297(13) 2.9715(15) 3.0751(15) 3.1378(12) 3.2448(15)	2.8404(10) 2.9262(10) 2.9652(10) 3.0662(9) 3.1317(9) 3.2382(10)	2.8320(11) 2.9197(11) 2.9840(10) 3.0622(10) 3.1495(11) 3.2726(12)	2.8528(10) 2.8894(11) 2.9762(11) 3.0647(11) 3.2495(12) 3.3161(12)	2.8483(5) 2.8839(5) 2.9703(5) 3.0579(5) 3.2428(5) 3.3093(6)	2.8153(12) 2.8575(12) 2.9875(12) 3.0817(12) 3.3265(12) 3.4549(13)	2.8156(14) 2.8563(13) 2.9857(12) 3.0810(12) 3.3269(13) 3.4500(14)	2.8387(17) 2.9218(11) 3.1699(12) 3.2905(17)
Br-Pb-Br	79.87(4) 81.08(3) 81.48(4) 81.59(4) 83.34(4) 87.48(4) 90.50(4) 90.44(4) 90.98(4) 107.69(4) 165.32(4) 170.72(3)	76.92(3) 79.92(3) 80.50(2) 81.05(2) 81.54(3) 81.57(3) 83.29(3) 87.59(3) 90.50(3) 90.40(3) 90.98(3) 95.13(3) 107.66(3) 113.60(3) 165.40(3) 166.00(2) 170.79(2)	79.73(3) 80.79(3) 83.30(3) 88.27(3) 90.24(3) 90.68(3) 107.65(3) 165.35(3) 171.53(2)	82.56(3) 82.68(2) 84.19(3) 87.84(3) 88.15(3) 93.77(3) 166.59(3)	82.552(13) 82.699(11) 84.195(13) 87.826(13) 88.161(13) 93.758(13) 166.595(10)	82.06(3) 85.98(3) 86.18(3) 89.87(3) 90.04(4) 92.23(3) 168.06(3)	81.97(4) 85.96(3) 86.21(4) 89.82(3) 90.06(4) 92.31(4) 167.99(3)	88.19(4) 91.32(5)
d_{N-Br}	3.4460(13) 3.4782(15) 3.4892(14) 3.5278(15) 3.6354(13)	3.4499(10) 3.4780(11) 3.4989(11) 3.5135(10) 3.6474(11)	3.4752(11) 3.4853(10) 3.4909(11) 3.5151(10) 3.6568(12)	3.4127(10) 3.4143(12) 3.5008(11) 3.5119(12) 3.5220(10)	3.4082(6) 3.4126(6) 3.4926(6) 3.5078(6) 3.5165(6)	3.3940(13) 3.4629(11) 3.4752(10) 3.5067(11) 3.6526(12)	3.3938(12) 3.4620(13) 3.4927(12) 3.4984(11) 3.6653(13)	3.4480(14) 3.5153(12)

Table S2. Main distances (standard deviation in parentheses) measured for (*S*)-**BuA**-$PbBr_3$, (*R*)-**BuA**-$PbBr_3$, *rac*-**BuA**-$PbBr_3$, (*S*)-**MBA**-$PbBr_3$, (*R*)-**MBA**-$PbBr_3$, (*S*)-**EBA**-$PbBr_3$, (*R*)-**EBA**-$PbBr_3$ and *rac*-**EBA**-$PbBr_3$

SHAPE program analysis[2]

Deviation considering 6-coordinated Pb
(CShM, Continuous Shape Measures)

	(*S*)-**BuA**-$PbBr_3$	(*R*)-**BuA**-$PbBr_3$	*rac*-**BuA**-$PbBr_3$	(*S*)-**MBA**-$PbBr_3$	(*R*)-**MBA**-$PbBr_3$	(*S*)-**EBA**-$PbBr_3$	(*R*)-**EBA**-$PbBr_3$	*rac*-**EBA**-$PbBr_3$
Deviation from Oh CShM	14.099	14.083	14.013	18.382	18.382	19.070	19.058	18.148

Deviation considering 5-coordinated Pb

	(*S*)-**BuA**-$PbBr_3$	(*R*)-**BuA**-$PbBr_3$	*rac*-**BuA**-$PbBr_3$	(*S*)-**MBA**-$PbBr_3$	(*R*)-**MBA**-$PbBr_3$	(*S*)-**EBA**-$PbBr_3$	(*R*)-**EBA**-$PbBr_3$	*rac*-**EBA**-$PbBr_3$
Deviation from C4v CShM	12.015	12.010	11.897	8.352	8.354	8.470	8.470	8.574
Deviation from D3h CShM	18.813	18.812	18.746	19.708	19.706	19.737	19.737	19.998

PL emission parameters as a function of octahedral distortion

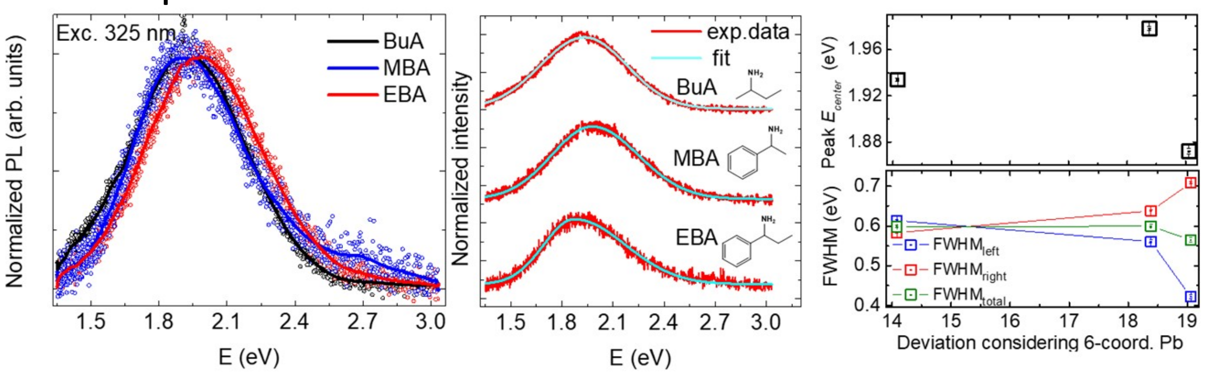

Figure S6: Left: PL spectra recorded using 3.81 eV excitation for (*R*)-**BuA**-$PbBr_3$, (*R*)-**MBA**-$PbBr_3$, (*R*)-**EBA**-$PbBr_3$ (points: experimental data, lines: smoothed spectra), middle: bi-gaussian fitting of the PL peaks, right: peak center position and FWHMs extracted from the fit as a function of the octahedral distortion determined using a $PbBr_6$ O_h model.

Time-resolved photoluminescence

Time-resolved PL studies were performed of the broadband emission for the (*R*)-**BuA**-$PbBr_3$ and (rac)-**BuA**-$PbBr_3$ samples, using 3.06 eV (405 nm) ps excitation and recording the PL decays as a function of detection wavelength. The Time-Correlated Single Photon Counting

2 a) M. Llunell, D. Casanova, J. Girera, P. Alemany, S. Alvarez, SHAPE, version 2.1, Universitat de Barcelona, Barcelona, Spain ; b) S. Alvarez, P. Alemany, D. Casanova, J. Cirera, M. Llunell, D. Avnir, Shape maps and polyhedral interconversion paths in transition metal chemistry, *Coord. Chem. Rev.*, 2005, **249**, 1693-1708.

measurements were performed in ambient conditions in a micro-PL setup in backscattering configuration. An avalanche photodiode was placed behind the exit slit of a monochromator used to filter the signal spectrally. The measurements were performed at 5 MHz laser repetition rate.

We observe a variation of the PL lifetime with detection energy for energies within the broad PL band (Fig. S7, S8). The PL decays show a multiexponential character which for the shortest time range can be well approximated by a biexponential with time constants in the ns range. The relative contribution of the shorter time decreases with decreasing emission energy and the transients are longer for the racemic compound. The short and long-time components obtained from the biexponential fits in the 0-10 ns range are 0.18 ns and 1.5 ns for the (*R*)-**BuA**-$PbBr_3$ sample and 0.43 ns and 3.59 ns for (rac)-**BuA-**$PbBr_3$, respectively. A similar biexponential character and increase of the lifetimes for lower emission energies has been previously observed for white light emitting thin 2 HOIP films and its observation was attributed to the presence of two different bands, originating from excitons trapped at different sites and characterized by different lifetimes.[3]Longer lifetimes for an achiral racemic PbBr based perovskite as compared to R,S enantiomers have been reported previously for a chiral **MPA** based HOIP[4] and explained by a lower energy barrier between the STE and FE state in the racemic compound, as well as a lower concentration of defects contributing to nonradiative losses . [4,5]

3 A. Yangui, D. Garrot, J. S. Lauret, A. Lusson, G. Bouchez, E. Deleporte, S. Pillet, E. E. Bendeif, M. Castro, S. Triki, Y. Abid, K. Boukheddaden, Optical Investigation of Broadband White-Light Emission in Self-Assembled Organic–Inorganic Perovskite $(C_6H_{11}NH_3)_2PbBr_4$, *J. Phys. Chem. C*, **2015**, 119, 23638-23647.

4 Y. Liu, C. Wang, Y. Guo, L. Ma, C. Zhou, Y. Liu, L. Zhu, X. Li, M. Zhang, G. Zhao New lead bromide chiral perovskites with ultra-broadband white-light emission, *J. Mater. Chem. C*, **2020**, 8, 5673-5680.

5 Z. Zhang, W.-H. Fang, M. V. Tokina, R. Long, and O. V. Prezhdo, 'Rapid Decoherence Suppresses Charge Recombination in Multi-Layer 2D Halide Perovskites: Time-Domain Ab Initio Analysis', *Nano Lett.*, vol. 18, no. 4, pp. 2459–2466, Apr. 2018, doi: 10.1021/acs.nanolett.8b00035

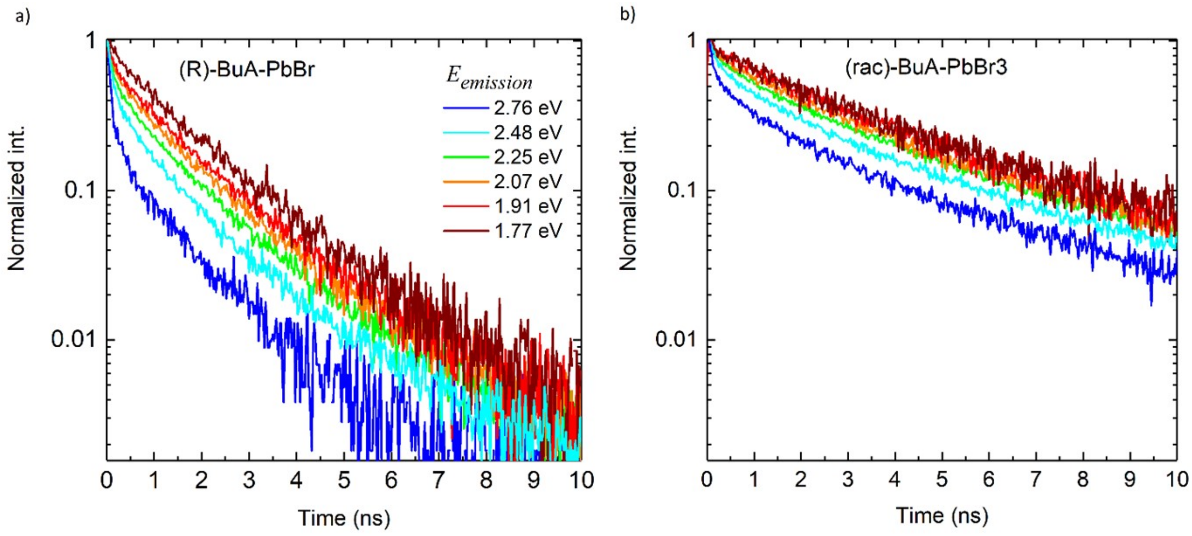

Figure S7: Time-resolved photoluminescence decays for 405 nm excitation and varying detection energy for a) (*R*)-**BuA**-$PbBr_3$ and b) (rac)-**BuA-**$PbBr_3$ in the short time range.

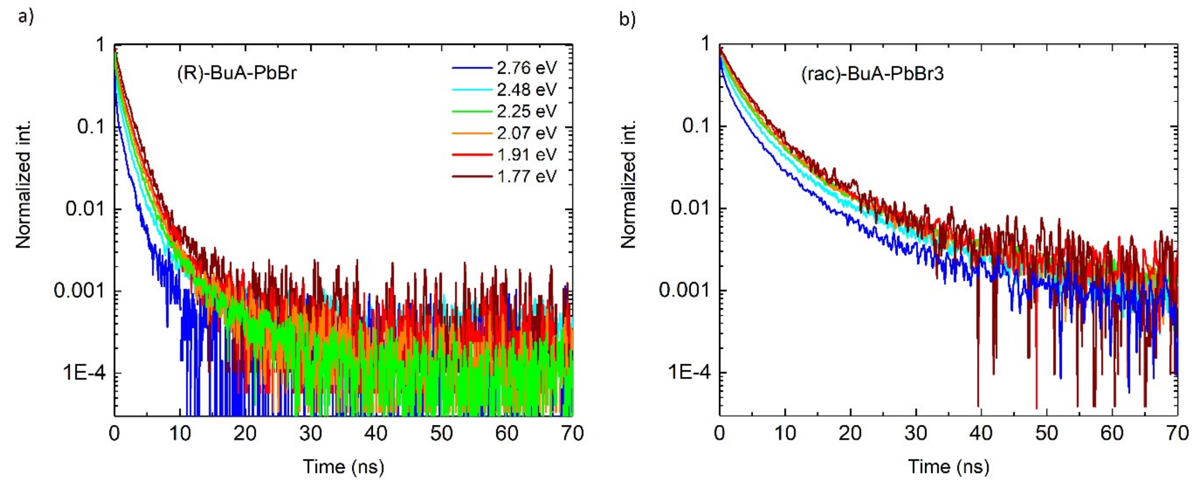

Figure S8: Time-resolved photoluminescence decays at 405 nm excitation for different detection energy for a) (*R*)-**BuA**-$PbBr_3$ and b) (rac)-**BuA-**$PbBr_3$ in the full recorded time range.

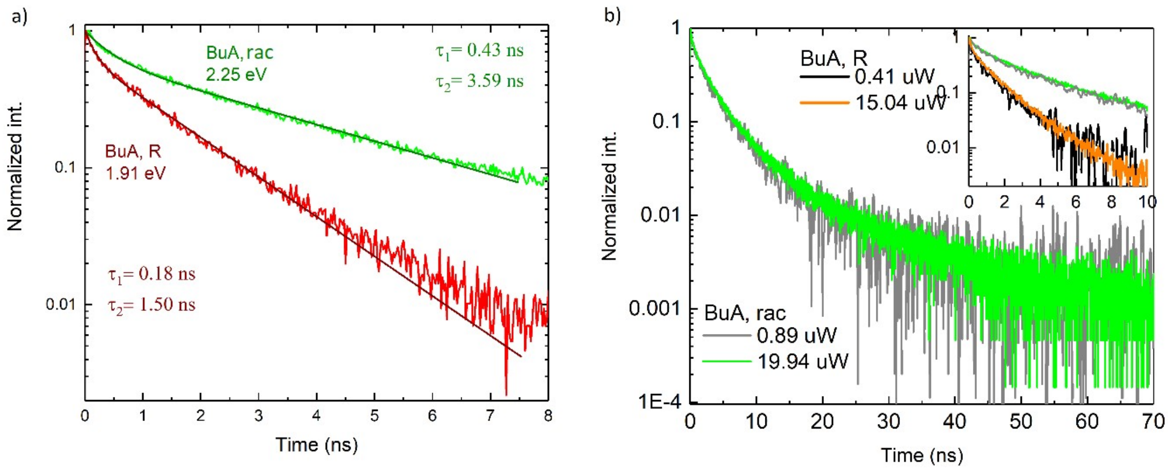

Figure S9: a) Biexponential fits of the decay curves recorded for the emission energy corresponding to the PL peak maximum for each compound at short times. The short and long-time components obtained from the biexponential fits in the 0-10 ns range are 0.18 ns and 1.5 ns for the (*R*)-**BuA**-$PbBr_3$ sample and 0.43 ns and 3.59 ns for (rac)-**BuA**-$PbBr_3$. b) Comparison of decay curves recorded for the emission energy corresponding to the PL peak maximum for both compounds at highest and lowest measured excitation power. Data is shown in the full time range only for sample (*R*)-**BuA**-$PbBr_3$, which has a significantly longer lifetime, for better clarity. The dynamics observed at energies corresponding to the maxima of the steady-state emission does not change for the investigated range of excitation powers, suggesting that neither carrier trapping at defects and other non-radiative loss channels nor Auger processes play a significant role in the PL dynamics.